1   **Direct Monitoring of Protein-Protein Inhibition Using Nano Electrospray**
2   **Ionization Mass Spectrometry**
3
4
5   Dragana Cubrilovic[1], Konstantin Barylyuk[1], Daniela Hofmann[2], Michal Jerzy Walczak [2], Martin
6   Gräber[3], Thorsten Berg[3], Gerhard Wider[2], Renato Zenobi[1*]
7
8   [1] Department of Chemistry and Applied Biosciences, ETH Zurich, 8093 Zurich, Switzerland
9   [2] Department of Molecular Biology and Biophysics, ETH Zurich, 8093 Zurich, Switzerland
10   [3] Institute of Organic Chemistry, University of Leipzig, 04103 Leipzig, Germany
11
12   [*] To whom correspondence should be addressed: Prof. Dr. Renato Zenobi, Department of
13   Chemistry and Applied Biosciences, ETH Zurich, 8093 Zurich, Switzerland. E-mail:
14   *zenobi@org.chem.ethz.ch*
15

19
20   **Abstract**

21   Dissociation of the TNF-alpha trimer caused by the small-molecule inhibitor SPD304 was
22   monitored using native ESI-MS and ion mobility spectrometry. Upon addition of inhibitor, our
23   data clearly indicates partial dissociation of the protein into dimers and monomers. The IMS-MS
24   analysis shows that dimeric ions have their own characteristic drift time distributions, which are
25   different from those of the dimer ions originating in the gas phase due to collision-induced
26   dissociation. We show that only one equivalent of the inhibitor binds to the trimeric form. We
27   also investigated inhibition of the heterodimer formation of the survival protein Bcl-x_L and cell
28   death-promoting regions of the proteins Bak and Bad, using the small inhibitors ABT737 and
29   ABT263. We found that the ABT737 is more potent compared to ABT263 in preventing the
30   heterodimerization between Bcl-x_L with Bak and Bad derived BH3 peptide. We could also
31   monitor the mode of binding, which in this case is competitive. These results indicate that native
32   ESI-MS can be widely used to study the inhibition of other relevant protein-protein interactions
33   (PPIs), and provide a good basis for further improvement and identification of small-molecules
34   PPI inhibitors.
35

36

37

40

Introduction

Protein-protein interactions (PPIs) are of fundamental importance in most biological processes - from intercellular function to programmed cell death. [1-3] The controlled disruption of PPIs with small-molecule inhibitors is of high interest in current drug discovery due to the large number of protein-protein interactions involved in signalling pathways related to cancer and many other human diseases. In the last decade, significant progress in the design and development of potential small inhibitors of PPIs has been made.[2, 4, 5] Therefore, understanding mechanisms of protein-protein disruptors can be used in several fields, e.g., in small molecule drug discovery, in order to design and optimize the novel potential therapeutics.

The conventional tools and methodologies for investigating PPIs include physico chemical methods such as X-ray crystallography, NMR spectroscopy, surface plasmon resonance (SPR), isothermal titration calorimetry (ITC), fluorescence spectroscopy, or biochemical methods. All these techniques have particular strengths and weaknesses in terms of sample consumption, throughput, dynamic range; some require immobilizing of one of the binding partners. [6-10]

Another powerful and increasingly utilized method to detect and characterize noncovalent interactions is nano electrospray ionization mass spectrometry (nanoESI-MS).[11-13] It was shown by many research groups that proteins in the gas phase are in a folded conformation, which is similar to the native conformation in solution, and that they are therefore able to bind inhibitors and provide a "snapshot" of the solution phase equilibrium.[14-17] In recent years, nanoESI-MS has become increasingly used in drug discovery, for the investigation of protein-ligand and protein-protein interactions.[17-21] This technique can address key questions about composition, stoichiometry, subunit interactions, and architectural organization of noncovalent complexes.[22]

The present work emphasizes the advantages of the native MS approach for direct monitoring of protein-protein inhibitions. Pioneering work in the detection of protein-protein interactions

66 inhibition via ESI-MS was carried out by Grygon and co-workers.[23] Beside the quantification of

67 protein-protein interactions it offers the possibility to directly visualize ligation states and

68 conformational changes upon addition of small disruptor molecule in solution.

69 In this work we have also applied ion mobility (IM) spectrometry, which is a gas-phase

70 separation tool comparable to electrophoresis in solution, and which can be combined with MS.

71 This is a technique that allows ions to be separated by a weak electric field in a gas environment

72 according to their mobility. [22] From the ion transport properties measurements, ion size

73 information can be generated. This results in an orientitatonally averaged ion-neutral collision

74 cross sections (CCS). [24] Recent studies show good correlation of many data sets between CCS

75 values based on IM measurements and X-ray or NMR data sets for the same proteins and

76 complexes in solution. Although these measurements are carried out in the absence of bulk water,

77 these studies suggest that IM data reflects condensed phase properties and can be used as a

78 technique for structural biology. Some of the recent reviews summarizing the developments of

79 IM-MS to rapidly measure changes in protein structure, oligomeric state, and binding

80 stoichiometry from complex mixtures are by Niu et al[24]., Hall and Robinson[25], and Konijnenberg

81 et al[26].

82 In this contribution we first investigated the alpha tumour necrosis factor (TNF-alpha), a cytokine

83 involved in systemic inflammation and in immune regulation, and therefore a therapeutic target

84 for many diseases. The known inhibitor SPD304 was used to induce dissociation of the trimeric

85 TNF-alpha, as monitored by nanoESI-MS.[27] In addition we performed ion mobility mass

86 spectrometry (IM-MS) experiments. NanoESI- and IM-MS results are in agreement, and, upon

87 ligand addition, show dissociation of the trimer into dimers and monomers. The IMS-MS analysis

88 shows that dimeric ions have their own characteristic drift time distributions, which are different

89 from dimer ions generated in the gas phase due to CID. Therefore dissociation occurs due to

90   SPD304-promoted dissociation of TNF-alpha trimers in solution. The mode of inhibitor binding

91   to the TNF-alpha was studied as well.

92   The second system investigated in this study is the interaction between the anti-apoptotic Bcl-2

93   family protein Bcl-x_L and two different pro-apoptotic binding partners, Bak and Bad. The pro-

94   apoptotic has similarity to the anti-apoptotic group in a single alpha helix called the BH3 region,

95   which is essential for binding to Bcl-x_L and also required for the proapoptotic effect.[28-33]

96   Heterodimerization between members of the Bcl-2 family proteins plays a key role in the

97   regulation of programmed cell death. In a first step we investigated the heterodimerization

98   between Bcl-x_L and the BH3 domain of Bak and Bad derived synthetic peptides, which bind with

99   high affinity in vitro; it had also been shown that the Bak BH3 peptide alone could induce

100   apoptosis in various cell lines.[30] Titration experiments at constant Bcl-x_L and different peptide

101   concentrations were first performed using nanoESI-MS. Results are in agreement with these from

102   other biophysical methods. In a second step, we investigated the recently introduced small BH3

103   mimetic inhibitors ABT737 and ABT263 that are designed to disrupt the above-mentioned

104   cancer-linked protein–protein interactions. These small-molecule inhibitors have been found to

105   occupy the BH3 binding groove of anti-apoptotic Bcl-2 family members, preventing them to

106   antagonize pro-apoptotic proteins and induce apoptosis, thereby enhancing programmed cell

107   death of cancer.[29,34] NanoESI-based results show that ABT737 prevent the heterodimerization of

108   Bcl-x_L-Bak as well as Bcl-x_L-Bad binding more efficiently compared to ABT263. We also

109   observed competition of the small molecule inhibitors with the BH3 derived peptide for the same

110   Bcl-x_L binding pocket, clearly indicating the mechanism of binding.

111   All nanoESI-MS based results obtained show that this technique is a valuable tool for

112   investigation of PPI inhibition. In addition to the quantification of binding strengths of PPIs, we

113   could gain information about stoichiometry, conformational changes, binding mechanism, and

114   relative binding strengths of the small PPI inhibitors from single-point measurements. Key

115   advantages of native MS are its simplicity (label-free measurements), selectivity (possibility of

116   using additional stages of MS combined with ion activation methods), sensitivity (low sample

117   consumption), and speed (mass spectra can be acquired in less than a minute).

118

119   **Experimental Section**

120   **Materials and Methods**

121   All solvents and caesium iodide (CsI) were purchased from Sigma Aldrich (Buchs, Switzerland).

122   The pET29 plasmid bearing the coding sequence of Bcl-x$_L$ (amino acids 1-209, Δ45-84) was a

123   kind gift from Prof. Ho Sup Yoon (Nanyang Technical University, Singapore). [31] The Bcl-xL

124   protein expression has been previously described.[28] The expression and purification protocol of

125   TNF-alpha (A.Corti).[35] was shortened and optimized by introduction of the N-terminal (His)$_6$-tag.

126   This allows for use of a Ni-NTA affinity purification step that significantly shortens the entire

127   purification protocol. Owing to the Ni-NTA step, troublesome and time-consuming hydrophobic

128   chromatography and desalting at 65% ammonium sulphate steps can be skipped. This results in a

129   higher yield of purified protein; the His-tag also allows immobilizing TNF on different media

130   (e.g. BiaCore chip or Ni-NTA beads). The BH3 peptide domains of the Bad

131   (NLWAAQRYGRELRRMSDK) and the Bak protein (GQVGRQLAIIGDDINR) were obtained

132   from Genscript (NJ, USA) and Anaspec (Fremont, USA), respectively. The small-molecule

133   inhibitor SPD304 was purchased from Cayman Chemicals (MI, USA), ABT737 and ABT263

134   from Selleckchem (TX, USA). Water was purified using a Milli-Q® Ultrapure water purification

135   system (Millipore, Barnstead, USA). Prior to mass spectrometric analysis the Bcl-x$_L$ protein

136   stock solution (224 μM) in 50 mM Hepes, 100 mM NaCl, 10 % glycerol, 1mM EDTA, 1mM

137   DTT, 0.1 % Nonidet-40 substitute (pH = 7.5) and the TNF-alpha protein stock solution in 50 mM

138   phosphate buffer, 100 mM NaCl, 2.5 mM EDTA (pH = 7.7) were desalted and buffer exchanged

139   (PD MiniTrap G-25, GE Healthcare, Buckinghamshire, UK) against the ammonium acetate

140   buffer. The stock solutions of Bad and Bak as well as small molecule inhibitors were dissolved in

141   DMSO at a concentration of 10 mM and further diluted in ammonium acetate to desired

142   concentration. All MS titration experiments were recorded under "native-like" conditions using

143   50 mM ammonium acetate buffer (pH = 7.7) for TNF-alpha-SPD304 and 300 mM (pH = 7.5) for

144   Bcl-x$_L$-peptide-inhibitor complex. To ensure the integrity of the protein complexes we kept the

145   pH of the ammonium acetate buffer the same as that of the buffer used for protein expression and

146   storage, which was previously optimized. In all experiments the DMSO concentration did not

147   exceed 1 % (v/v). For TNF-alpha denaturation, ZipTip columns containing C$_4$-resin (Millipore,

148   Molsheim, France) were used. The exact TNF-alpha and Bcl-x$_L$ concentration was determined

149   using a UV spectrometer (Genesys 10S UV-VIS, ThermoScientific, Bremen, Germany) by

150   measuring the absorbance at 280 nm.

151

152   **Mass spectrometry**

153   NanoESI-MS analyses were performed with a hybrid quadrupole time-of-flight mass

154   spectrometer (Q-TOF ULTIMA, Waters/Micromass, Manchester, UK) in positive ion mode. The

155   instrument was controlled via the MassLynx software (version 4.0). Sample solutions were

156   directly infused with gold/palladium-coated borosilicate glass offline nanoESI emitters (Thermo

157   Fisher Scientific, Reinach, Switzerland) using a commercial nanoESI ion source

158   (Waters/Micromass, Manchester, UK). The capillary voltage was set to 1.8 kV and a gentle

159   backing pressure of 0.3-0.5 bar was applied to assist the liquid sample flow. The source

160   temperature was kept at room temperature. Instrumental conditions had to be adjusted in order to

161   get narrow peaks of the detected ions without dissociating the noncovalent complex. The precise

5

162   settings have an influence on the peak shape: due to adduct formation with salt and buffer

163   molecules from the spray solution, peaks might be broadened. The mass spectrometer was run

164   with the following gentle desolvation parameters: the cone and first ion tunnel RF1 voltages,

165   parameters that control the kinetic energy of the ions in the source region of the mass

166   spectrometer, were set to 50 and 50 V for Bcl-x_L; and 70 and 60 V for TNF-alpha experiments,

167   respectively. After this stage, the ion beam passed a hexapole collision cell filled with argon

168   (purity 5.0, PanGas, Zurich, Switzerland). The collision energy offset was used to optimize

169   desolvation and set to 22 V. The pressure in the source was increased to 5.5 mbar, using a

170   "speedivalve" (Edwards Ltd., Sussex, UK) connected between the rotary pump and source

171   pumping line. All instrument parameters used (e.g. capillary voltage, cone voltage, RF1 voltage,

172   collision energy) were carefully adjusted and optimized to be as soft as possible for all

173   investigated protein-complexes. Collision-induced dissociation (CID) used for TNF-alpha

174   MS/MS experiments were performed by adjusting the acceleration collision energy (CE) offset

175   until full dissociation of the parent ions was achieved. The ion transmission was optimized for a

176   m/z range between 100 and 9,000 Da for TNF-alpha, and 100-5,000 Da for Bcl-x_L. The scan time

177   and interscan times were 1 and 0.2 sec, respectively.

178   IMS-MS experiments were performed on the Synapt G2-S HDMS (Waters, Manchester, UK).

179   Ions were produced by a commercial NanoLock Spray ionization source (Waters, Manchester,

180   UK) using offline capillary emitters (see above). A capillary voltage of 0.8-1.3 kV and a backing

181   pressure of 0.25-0.3 bar were applied to generate the nano-electrospray. The sampling cone

182   voltage and the source offset were set to 20 and 80 V, respectively. The traveling-wave ion

183   guides were tuned to minimize unwanted fragmentation of ions during ion transfer, trapping, ion

184   mobility separation, and mass analysis. For instance, the trap DC bias, helium cell DC offset, and

185   IMS bias were lowered to 40, 30 and 0.5 V, respectively. The trap gas flow was increased to

6

186   5.5 ml min^{-1} to facilitate transmission of high-*m/z* ions. The trap and transfer collision energies

187   were set to 10 and 5 V, respectively, and trap and transfer CID was induced by increasing the

188   corresponding voltage offsets. Ion mobility separations were carried out using IMS wave velocity

189   (WV) ramping of 1600 to 200 m s^{-1} (unless specified differently) and wave height (WH)

190   amplitude of 40 V. Nitrogen (purity 5.0, PanGas, Zurich, Switzerland) was used as IMS buffer

191   gas. The spectra were acquired in the range of *m/z* 50-8000 using scan time of 2 s and interscan

192   delay of 0.01 s. Typically, at least 50 scans were combined to produce a spectrum.

193   Calibration of the mass spectrometry instrument was performed using caesium iodide (CsI)

194   clusters. CsI was dissolved in water/2-propanol (1/1, v/v) at a concentration of 2 μg/μL.

195   **Data processing**

196   Before data processing, each mass spectrum was smoothed (Savitzky-Gollay smooth) with the

197   MassLynx 4.0 software (Waters, UK). For the dissociation constant (K_D) determination of the

198   Bcl-x$_L$-Bad and Bcl-x$_L$-Bak complexes the measured relative peak heights (I) were used. The

199   peak height ratio (R) of the Bad- and Bak-bound Bcl-x$_L$ complex (P·L) to bare protein (P), R = I

200   (P·L)/ I (P), was calculated for each spectrum. For this determination, all charge states were taken

201   into account. The ratio of the sum of all detected complex species divided by the sum of the free

202   protein was determined. The experimentally calculated relative peak heights were plotted versus

203   the total added Bad or Bak concentration. The equation derived by Daniel et al.[12] was used to

204   determine the K_D values from fitting a titration curve:

$$\frac{I(P \cdot L)}{I(P)} = \frac{1}{2}\left(-1 - \frac{[P]_0}{K_D} + \frac{[L]_0}{K_D} + \sqrt{4\frac{[L]_0}{K_D} + \left(\frac{[L]_0}{K_D} - \frac{[P]_0}{K_D} - 1\right)^2}\right)$$

205

206   The K_D calculations and the fitting of the titration curves were performed using the MATLAB

207   software (2010a, The MathWorks, Natick, MA, USA).

208

7

Results and Discussion

NanoESI-MS analysis of TNF-alpha

Prior to the addition of the inhibitor to TNF-alpha, the proper instrumental conditions had to be adjusted to preserve the trimeric protein structure. Therefore the trimeric human TNF-alpha was analysed under denaturing and "native" conditions using the Q-TOF ULTIMA. In **Figure SI1 (Supporting Information)**, nanoESI mass spectra for a solution of denatured and native TNF-alpha are shown. The first spectrum measured under denatured conditions generates a broad charge state distribution. Under this condition the completely unfolded monomer that appears in the lower *m/z* range is detected. In contrast, **Figure SI1B** displays the spectrum under "native-like" conditions in 50 mM ammonium acetate and 1 % DMSO at pH = 7.7. The observed narrow charge state distribution, predominantly + 11, + 12, + 13, is typical for non-denaturing conditions, and is consistent with a compact conformation in solution. In addition to the trimeric TNF-alpha ions, we can observe minor monomeric peaks at + 7, + 6, as well. Many studies have demonstrated that the charge state distribution depends on the protein conformation in solution.[36-38] Native nanoESI-MS analysis of the protein is relevant, since proper TNF-alpha folding is crucial for the later interaction with the inhibitor in solution.

In addition we performed CID experiments in order to confirm the trimeric TNF-alpha assembly and gain additional information about the protein stability in the gas phase. For the MS/MS measurements the +14 trimeric ions were selected and dissociated during transmission through the mass spectrometer. For this, the CE offset was varied in 10 V steps from 15 to 100 V, until the selected trimeric ions were completely dissociated. In **Figure SI2** two different CID spectra at a CE offset of 30 and 100 V are shown. Dissociation of the precursor ions yielded the dimeric and monomeric protein ions. These CID experiments provide additional evidence for the trimeric TNF-alpha assembly. In should be mentioned that different charge state distribution are generated

234 in the absence and in the presence of 1% DMSO. This effect is described in the next subsection

235 more in detail.

236

237 **Monitoring the disruption of the TNF-alpha trimer due to the binding of the inhibitor**

238 **SPD304 by nanoESI- and ion mobility-MS**

239 SPD304 has previously been identified as potent inhibitor against TNF-alpha. We monitored the

240 influence of SPD304 on TNF-alpha using nanoESI- and ion mobility-MS. At this point it is

241 noteworthy to state that the described experiments were run in 1 % DMSO (v/v). It has been

242 shown that this DMSO amount will not significantly influence the binding of the small molecule

243 to the protein as observed by nanoESI-MS.[39] However, it is still necessary to perform

244 experiments in the presence and in the absence of DMSO. This should be considered in order to

245 properly evaluate any possible conformational difference, resulting in a different charge state

246 distribution, of the complex and the bare or dissociated protein. Also, DMSO may lead to partial

247 dissociation of the protein. **Figure 1** illustrates IMS-MS analysis of TNF-alpha under "native

248 ESI-MS" conditions. The shown results should provide additional structural information based on

249 the separation of gas-phase ions based on their differential transport through an environment of

250 inert neutrals.[24] We show the 2D IMS drift time vs. m/z plots with corresponding mass spectra

251 and drift time distributions. We first performed experiments using a 4.5 μM TNF-alpha solution

252 in 75 mM ammonium acetate buffer at pH = 7.7 and the same protein concentration in the

253 presence of 1 % (vol.) DMSO. In the presence of 1% DMSO, an overall charge state reduction

254 can be observed; +11, +12, +13 compared to +13, +14, +15, +16. The appearance of a small

255 amount of the monomers is also observed in the presence of DMSO. The trimeric form is

256 compact in both cases. As a next experiment, we have investigated the influence of the inhibitor

257 by adding 100 μM SPD304 to 4.5 μM trimeric TNF-alpha in 75 mM ammonium acetate solution

258 at pH = 7.7 in 1 % DMSO. The same charge state distribution is detected for the TNF-alpha upon

259   inhibitor addition. Again, three different compact charge states representing the TNF-alpha trimer

260   are observed. The appearance of dimer ions and the increase of monomer peak intensities is

261   clearly seen, indicating the dissociation of the trimeric protein form in solution. The advantage of

262   IM-MS in this case is the clear separation of dimer and trimer ions due to their different drift

263   times.

264   The peak maxima in the drift time distributions are represented with the respective bin numbers.

265   As can been seen in **Figure 1,** the +13 charge state of the trimeric protein appears in all three

266   cases (without DMSO, with DMSO, and upon ligand binding). The +13 charge state shows the

267   same drift time distribution in all three cases. These results indicate clearly that the dissociation

268   upon ligand addition already happens in solution and not due to partial dissociation of the trimer

269   in the gas phase.

270   Under this aspect, we have also investigated the dependence of the drift time distribution of the

271   TNF-alpha trimer 13+ ion on the trap collision energy applied (Figure SI3). This charge state was

272   chosen since it is generated in all three cases (with and without DMSO and in the presence of the

273   inhibitor). The selected 13+ ions were interrogated by changing the trap collision voltage in the

274   ion trap just prior to the mobility cell. The increased voltage accelerates the ions such that they

275   encounter neutral gas molecules with greater kinetic energy in the ion trap. Nearly identical

276   collision-induced unfolding profiles registered for the TNF-alpha T13+ ion electrosprayed from

277   various solution conditions (buffer, 1 % DMSO, 1 % DMSO + 100 μM ligand) is observed. The

278   drift time distribution of T13+ ion is narrow and unimodal in all three cases, with the peak

279   maximum in bins 85-86 up to a trap collision energy offset of 30 V. At a collision energy of 40

280   V, unfolding starts, which is manifested by a slight broadening of the drift time distribution and a

281   minor shift of the peak towards shorter drift time, due perhaps to a gas-phase collapse of the

282   trimer. As the collision energy increases to 50 and 60 V, the drift time distribution broadens

283 dramatically, shifts towards higher drift times, and becomes multimodal, with several more or

284 less overlapping peaks. Dissociation into monomer and dimer ions with asymmetric charge

285 partitioning is observed simultaneously in mass spectrum (data not shown). At high trap collision

286 energies, the drift time distribution coalesces into a single peak at bin 108. This behavior

287 resembles a two-state, all-or-none protein-unfolding behavior. [40-42] The most important

288 conclusion is that the behavior of T13+ is the same in all three cases, i. e., that there are no

289 stabilizing or de-stabilizing effects found in the gas phase when the protein is incubated with

290 DMSO or ligand.

291 In **Figure 2,** the IMS-MS analysis of TNF-alpha ions produced under "native ESI" conditions

292 from 4.5 μM protein solution in 75 mM ammonium acetate buffer (pH 7.7) containing 1 % (vol.)

293 DMSO and 100 μM SPD304 is shown. The sample is analysed at various transfer collision

294 energy offsets. The ions were interrogated by changing the transfer collision voltage in the

295 transfer region just after the mobility cell. TNF-alpha dimer ions D8+, D9+, and D10+ are

296 present even at low transfer collision energy offsets (**Fig. 2A and B**). At high collision energy

297 offsets (**Fig. 2C and D**), collision-induced dissociation (CID) of TNF-alpha ions occurred in the

298 transfer region of the mass spectrometer, after IMS separation. Thus, fragment ions have the

299 same drift time, as the respective parent. The D8+, D9+, and D10+ ions have their own

300 characteristic drift time distributions, which are different from those of the dimer ions originating

301 in the gas phase due to CID. Therefore, D8+, D9+, and D10+ ions must have been present in the

302 sample prior to IMS-MS analysis, i.e. they occurred due to SPD304-promoted dissociation of

303 TNF-alpha trimers in solution.

304 In addition, we have performed nanoESI-MS measurements on the Q-TOF ULTIMA. **Figure SI4**

305 shows the influence of adding of 100 μM SPD304 to 4.5 μM trimeric TNF-alpha on the nanoESI

306 mass spectra in 50 mM ammonium acetate solution at pH = 7.7 in 1 % DMSO. Interestingly, here

11

307   we can observe a wider charge state distribution in the spectrum compared to the above-

308   mentioned results. Additional charge states, the +14, +15 and +16 ions, are generated compared

309   to the spectrum without inhibitor (see **Figure SI1B**). However, it would be quite speculative to

310   state that this shift in charge state distribution towards lower m/z indicates a "less compact"

311   trimeric protein structure in the presence of SPD304. This "more open" trimeric form may go

312   hand in hand with a partial dissociation of the protein into dimers and monomers, which indicates

313   a conformational change in the protein structure. The observation that the dimer abundance is

314   lower compared to monomers is probably due to a lower ionization efficiency of the dimeric

315   form. A very interesting result is that TNF-alpha forms a noncovalent complex by binding one

316   inhibitor molecule. No ligation states with two or three ligands were detected.

317   A X-ray structure reveals that a one equivalent of the inhibitor molecule displaces a subunit of

318   the trimer and leads to the formation of a dimeric protein form. Biophysical experiments as well

319   as biochemical and cell-based assays have shown that the inhibitor was capable to dissociate

320   TNF-alpha trimer in solution and also the interaction between intact trimeric protein, which lead

321   to subunit dissociation.[27] The ESI-MS and IM-MS results are in agreement with this structural

322   data, but complement them in the sense that we gain additional insight into inhibitor binding to

323   TNF-alpha.

324

325   **K_D determination of the Bcl-x$_L$·Bak and Bcl-x$_L$·Bad complexes by the nanoESI-MS titration**
326   **method**

327

328   As a second system we investigated the heterodimerization between members of the Bcl-2 family

329   of proteins, which is very important in regulating programmed cell death. The subsequent

330   influence of small molecule disruptors on these interactions was monitored as well. In the first

331   step, before addition of small disruptors ABT737 and ABT263, we carried out measurements

332   with Bcl-xL (amino acids 1-209, Δ 45-84) in complex with the synthetic peptides of the Bak- and

333 Bad BH3 domain. **In Figure 3A** the nanoESI mass spectra of the bare protein in the presence and

334 in the absence of Bak in 300 mM aqueous ammonium acetate at pH = 7.5 are shown. A narrow

335 charge state distribution, predominantly 7+, 8+ ions, appears at fairly high m/z. This is

336 characteristic for native conditions, and consistent with a compact conformation of Bcl-x_L in

337 solution. In order to determine the dissociation constant via the titration method, a set of nanoESI

338 experiments was performed with increasing Bak concentrations ranging from 0.5 to 3 μM, at a

339 constant Bcl-x_L concentration. **Figure 3A** displays representative nanoESI spectra obtained for

340 the Bcl-x_L•Bak complex at three different ligand concentrations. As expected, increased complex

341 signal intensity was observed with higher total Bak concentration. At 3 μM Bak concentration,

342 full complexation was reached (data not shown). Titration experiments for Bcl-xL•Bak binding

343 over a range of concentrations were performed. We can detect different complex/free protein

344 ratios for different charge states. This phenomenon is well known and has already been

345 mentioned for different noncovalent complexes, although no clear explanation can be found in

346 the literature. [6, 22, 43] In order to determine the K_D we took the abundance (peak intensities) of all

347 detected complex and protein ions into account. The titration curve is shown in **Figure 3B**. The

348 signal ratio of the detected complex and the sum of the free protein and the complex signal was

349 plotted against the total ligand concentration (L_0). The K_D determined by a set of titration

350 experiments was 314 ± 35 nM. This value is in very good agreement with other values

351 determined for Bcl-x_L•Bak in solution. In the literature, K_D values of 480 nM and 340 nM using a

352 fluorescence polarization-based competition assay were obtained.[31,32]

353 For Bcl-x_L in complex with the Bad BH3 derived peptide we performed titration experiments as

354 well. The charge state distribution is comparable with that obtained for Bcl-x_L•Bak. However,

355 higher Bad concentrations were needed to reach full complexation. Therefore the titration

356 experiments were performed from 2 to 20 μM (data not shown). The K_D determined for Bad

13

357   binding to BcL-xL is 4.45 ± 0.3 μM. Depending on the length of the synthetic Bad peptide K_D

358   values ranging from 50 μM to the low nanomolar range were reported using fluorescence

359   polarization competition assay. [44]

360   For the Bcl-x_L•Bak and Bcl-x_L•Bad disruption with ABT737 and ABT293, we performed the

361   experiments at concentrations where mainly the complex peak is observed in the spectrum. In

362   case of Bcl-x_L•Bak, the ratio was 1:1 (eq) and for the Bcl-x_L•Bad binding 1: 6.6 (eq). The

363   experiments are described in detail in the next section.

364

365   **Monitoring the Bcl-x_L-Bak and Bcl-x_L-Bad inhibition using small disruptors ABT737 and**
366   **ABT293**
367
368
369   We used native MS to directly monitor the inhibition of the Bcl-x_L-Bak and Bcl-x_L-Bad

370   heterodimers in the presence of the small inhibitors ABT737 and ABT263. These compounds

371   were shown to inhibit binding of peptide and induce apoptosis. [34]

372   Experiments with the small disruptor ABT737 of the Bcl-xL•Bak heterodimer were first carried

373   out. In **Figure 4A** the spectra of 3 μM Bcl-x_L in complex with 3 μM Bak (full complexation

374   reached), in the presence at different ABT737 concentrations ranging from 1.25 to 12.5 μM are

375   shown. With higher inhibitor concentration we can clearly monitor the increasing disruption of

376   the Bcl-x_L•Bak interaction. Upon addition of the small inhibitor the disrupted Bcl-x_L•Bak

377   complex generates additional peaks of the bare Bcl-x_L protein and a Bcl-x_L•ABT737 complex.

378   This observation gives us additional information about the mechanism of binding of the ABT737,

379   which is in this case is competitive. The small disruptor ABT737 is able to displace the Bak

380   derived peptide from the BH3 binding pocket of Bcl-x_L. No peaks where all three species form a

381   complex were detected, which confirm our interpretation of a competitive mechanism. In a recent

382   study it was described that ABT binds to the BH3 pocket of Bcl-x_L, breaking its hold on Bak. [29,34]

383 At 12.5 μM ABT737 the major +8 peak is Bcl-x$_L$ in complex with ABT737, only a minor

384 undisrupted +8 heterodimer peak remains.

385 For the native MS measurements of the Bcl-x$_L$•Bak disruption in the presence of the small

386 inhibitor ABT263, the same instrument conditions were used. In **Figure 4B** the spectra of 3 μM

387 Bcl-x$_L$ in complex with 3 μM Bak in the presence at different ABT263 concentration between

388 6.25 μM and 25 μM are shown. The mode of binding is, as in the previous case, competitive,

389 although a significant difference in the inhibition of PPI compared to ABT737 was detected. In

390 order to disrupt half of the heterodimer, 17.5 μM of ABT263 had to be present in solution. As

391 shown in **Figure 5**, 6.25 μM ABT737 disrupt three times more Bcl-x$_L$•Bak complex compared to

392 ABT263 at the same concentration.

393 This observation lets us conclude that ABT263 is a less active inhibitor compared to ABT737.

394 These data are consistent with those generated in a TR-FRET assay, which also indicate that

395 ABT737 is more active than ABT26.[34] In addition, the in vitro efficacies of ABT737 and

396 ABT263 were studied in a recent study. The authors have shown that ABT737 is more active

397 than ABT263 in inducing apoptosis in chronic lymphocytic leukemia (CCL) cells, because

398 ABT263 was more strongly bound by albumin compared to ABT737, which accounted for the

399 differential sensitivity of CLL cells. [45] However, the activities in our assay using purified protein

400 are not affected by albumin binding.

401 In a second step, we also studied the influence of ABT737 and ABT263 on the Bcl-x$_L$•Bad

402 interaction. For this the experiments with the small inhibitors with 3 μM Bcl-xL in complex with

403 20 μM Bad were performed. **Figure 5** displays nanoESI spectra at different ABT737 and

404 ABT263 concentrations. Again, with higher inhibitor concentration the stronger disruption of the

405 Bcl-x$_L$•Bad interaction is detected. The disrupted Bcl-x$_L$-Bad complex dissociates into ions

406 representing the bare Bcl-xL protein and the Bcl-xL•ABT737 or Bcl-xL•ABT263 complexes. We

15

407   found again that the ABT737 is more potent compared to ABT263 in preventing the

408   heterodimerization between Bcl-xL and Bad derived BH3 peptide in solution. To completely

409   dissociate the dimerization, a 2.5 times higher concentration of ABT263 was required,

410   corresponding to the18 μM ABT263 and 7 μM ABT737 inhibitor concentration.

411   The heterodimer ratios (Bcl-xL-Bak/ Bcl-xL or Bcl-xL-Bad/ Bcl-xL)) upon addition of the total

412   ABT263 and ABT737 concentration are plotted in **Figure 6**. Compared to the Bcl-x_L•Bak, no

413   significant difference in the inhibitor efficiency is observed in preventing the Bcl-x_L•Bad

414   interaction; ABT737 and ABT263 seem to have a very similar influence in disrupting both

415   investigated heterodimers. For the Bcl-x_L•Bad disruption with ABT263, no significant difference

416   in dissociation of the heterodimer with lower ABT263 concentration is observed. Therefore less

417   data points are plotted compared to other three investigated systems. We could show that the

418   native MS approach is suitable to directly monitor not only PPI inhibition, but also the relative

419   binding strengths and the nature of binding.

420
421   **Conclusions**
422
423   In this study we investigated the inhibition of protein-protein interactions using nanoESI-MS. As

424   a first system we investigated the dissociation of the trimeric TNF-alpha in the presence of the

425   inhibitor SPD304. Ion mobility experiments were performed as well. The inhibitor promotes

426   subunit disassembly of the trimeric form into monomers and dimers. Only one molecule inhibitor

427   binds to the trimeric TNF-alpha. The SPD304-promoted dissociation into dimers ions must have

428   been present in the sample prior to IMS-MS analysis, since the dimeric ions have their own

429   characteristic drift time distributions, which are different from those of dimer ions originating in

430   the gas phase due to CID.

431 As a second system we investigated the inhibition of the heterodimer formation of the survival

432 protein Bcl-x$_L$ and death-promoting regions of proteins Bak and Bad. Recently developed small-

433 molecule inhibitors for the above-mentioned interaction, ABT737 and ABT263, were used to

434 detect the disruption of the heterodimers. In the first step we determined the dissociation

435 constants of the Bcl-x$_L$ in complex with Bak or Bad derived peptide domain applying titration

436 method. The ratio of the protein-peptide wherein the complex peak was generated was used for

437 further experiments with small inhibitors. We found that ABT737 is more active inhibitor

438 compared to ABT263 in disrupting the heterodimerization between Bcl-x$_L$ and Bak and also Bad

439 derived BH3 peptide. The small disruptor ABT737 as well as ABT263 is able to displace the Bak

440 and Bad derived peptide from the BH3 mainly hydrophobic pocket of the Bcl-xL. This

441 observation indicates a competitive mode of binding.

442 The nanoESI-based results for both investigated systems are in agreement with our biophysical

443 methods in terms and can therefore be used as a suitable/appropriate technique for studying PPI

444 inhibition. Due to the advantages of the nanoESI approach in terms of speed, absence of label and

445 sensitivity, we believe that can be widely used for better understanding and development of small

446 inhibitors of PPIs. This method allows the monitoring of ligation states, provide information of

447 mechanisms, on stoichiometry and relative binding potency.

448
449

455
456

457
458
459

References

(1)   Arkin, M. R. Wells, J. A. *Nat. Rev. Drug Discov.,* **2004**, *3*, 301.

(2)   Wilson, J. A. *Chem Soc Rev.,* **2009**, *38*, 3289.

(3)   Valkov, E. Sharpe, T. Marsh, M. Greive, S. Hyvönen, M. In *Fragment-Based Drug Discovery and X-Ray Crystallography*, Springer Berlin Heidelberg, 2012, Vol. 317.

(4)   Gasilova, N. Nazabal, A. In *Chemical Proteomics.*, Drewes, G., Bantscheff, M., Eds.; Humana Press, 2012, Vol. 803.

(5)   Vassilev, L. T. Vu, B. T. Graves, B. Carvajal, D. Podlaski, F. Filipovic, Z.; Kong, N. Kammlott, U. Lukacs, C. Klein, C. Fotouhi, N. Liu, E. A., *Science* **2004**, *303*, 844.

(6)   Kitova, E. N. El-Hawiet, A. Schnier, P. D. Klassen, J. S. *J. Am. Soc. Mass Spectrom.,* **2012**, *23*, 431.

(7)   Maple, H. J. Garlish, R. A. Rigau-Roca, L. Porter, J. Whitcombe, I. Prosser, C. E. Kennedy, J.; Henry, A. J.; Taylor, R. J.; Crump, M. P.; Crosby, J., *J. Med. Chem.* **2012**, *55*, 837.

(8)   Cooper, M. A. *Nat. Rev. Drug Discov.,* **2002**, *1*, 515.

(9)   de Azevedo, W. F. Dias, R. *Curr. Drug Targets,* **2008**, *9*, 1071.

(10) Meyer, B. Peters, T. *Angew. Chem. Int. Ed.,* **2003**, *42*, 864.

(11) Hofstadler, S. A. Sannes-Lowery, K. A. *Nat. Rev. Drug Discov.,* **2006**, *5*, 585.

(12) Daniel, J. M. McCombie, G. Wendt, S. Zenobi, R. *J. Am. Soc. Mass Spectrom.,* **2003**, *14*, 442.

(13) Tjernberg, A. Carno, S. Oliv, F. Benkestock, K. Edlund, P. O. Griffiths, W. J. Hallen, D., *Anal. Chem.,* **2004**, *76*, 4325.

(14) Sharon, M. V. Robinson, C. *Curr. Proteomics,* **2011**, *8*, 47.

(15) Lorenzen, K.; Duijn, E. V., *Curr. Protoc. Protein Sci.*; John Wiley & Sons, Inc., **2001**. 17.12.1-17.12.17.

(16) Breuker, K. McLafferty, F. W. *Proc. Natl. Acad. Sci. .,* **2008**, *105*, 18145.

(17) Zhang, S. Van Pelt, C. K. Wilson, W. D., *Anal. Chem.* **2003**, *75*, 3010.

(18) Zhang, J.; McCombie, G.; Guenat, C.; Knochenmuss, R. *Drug Discov. Today,* **2005**, *10*, 635.

(19) Deng, G. J. Sanyal, G. *J. Pharm. Biomed. Anal.,* **2006**, *40*, 528.

(20) Loo, J. A. *Mass Spectrom. Rev.,* **1997**, *16*, 1.

(21) Loo, J. A. Hu, P. McConnell, P. Mueller, W. T., *J. Am. Soc. Mass Spectrom.* **1997**, *8*, 234.

(22) Atmanene, C. Petiot-Bécard, S. Zeyer, D. Van Dorsselaer, A. Vivat Hannah, V. Sanglier-Cianfèrani, S. *Anal. Chem.,* **2012**, *84*, 4703.

(23) Davidson, W. Hopkins, J. Jeanfavre, D. Barney, K. Kelly, T. Grygon, C. *J. Am. Soc. Mass Spectrom.,* **2003**, *14*, 8.

(24) Niu, S. Rabuck, J. N. Ruotolo, B. T., *Curr. Opinion Chem. Bio.,* **2013**, *17*, 809.

(25) Hall, Z. Robinson, C. V. *J. Am. Soc. Mass Spectrom.,* **2012**, *23*, 1161.

(26) Konijnenberg, A.; Butterer, A.; Sobott, F. *Biochimica et Biophysica Acta (BBA) - Proteins and Proteomics ,* **2013**, *1834*, 1239.

(27) He, M. M. Smith, A. S. Oslob, J. D. Flanagan, W. M. Braisted, A. C. Whitty, A. Cancilla, M. T. Wang, J. Lugovskoy, A. A. Yoburn, J. C. Fung, A. D. Farrington, G. Eldredge, J. K. Day, E. S.; Cruz, L. A. Cachero, T. G. Miller, S. K. Friedman, J. E. Choong, I. C. Cunningham, B. C., *Science,* **2005**, *310*, 1022.

506   (28)   Gräber, M. Hell, M. Gröst, C. Friberg, A. Sperl, B. Sattler, M. Berg, T., *Angew. Chem.*
507   *Int. Ed.,* **2013**, *52*, 4487.
508   (29)   Oltersdorf, T. Elmore, S. W. Shoemaker, A. R. Armstrong, R. C. Augeri, D. J. Belli, B. A.
509   Bruncko, M. Deckwerth, T. L. Dinges, J. Hajduk, P. J. Joseph, M. K. Kitada, S.
510   Korsmeyer, S. J. Kunzer, A. R. Letai, A. Li, C. Mitten, M. J. Nettesheim, D. G. Ng, S.
511   Nimmer, P. M. O'Connor, J. M. Oleksijew, A. Petros, A. M. Reed, J. C. Shen, W. Tahir,
512   S. K. Thompson, C. B. Tomaselli, K. J. Wang, B. Wendt, M. D. Zhang, H. Fesik, S. W.
513   Rosenberg, S. H., *Nature* **2005**, *435*, 677.
514   (30)   Zhang, H. Nimmer, P. Rosenberg, S. H. Ng, S.-C. Joseph, M. *Anal. Biochem.,* **2002**, *307*,
515   70.
516   (31)   Petros, A. M., Medek, A., Nettesheim, D. G., Kim, D. H., Yoon, H. S., Swift, K.,
517   Matayoshi, E. D., Oltersdorf, T., Fesik, S. W., *Proc. Natl. Acad. Sci. ,* **2001**, *98*, 3012.
518   (32)   Sattler, M. Liang, H. Nettesheim, D. Meadows, R. P. Harlan, J. E. Eberstadt, M. Yoon, H.
519   S. Shuker, S. B. Chang, B. S. Minn, A. J. Thompson, C. B. Fesik, S. W., *Science* **1997**,
520   *275*, 983.
521   (33)   Muchmore, S. W. Sattler, M. Liang, H. Meadows, R. P. Harlan, J. E. Yoon, H. S.
522   Nettesheim, D. Chang, B. S. Thompson, C. B. Wong, S.-L. Ng, S.-C. Fesik, S. W., *Nature*
523   **1996**, *381*, 335.
524   (34)   Tse, C. Shoemaker, A. R. Adickes, J. Anderson, M. G. Chen, J. Jin, S. Johnson, E. F.
525   Marsh, K. C. Mitten, M. J. Nimmer, P. Roberts, L. Tahir, S. K. Xiao, Y. Yang, X. Zhang,
526   H.; Fesik, S. Rosenberg, S. H. Elmore, S. W. *Cancer Res.,* **2008**, *68*, 3421.
527   (35)   Curnis, F. Corti, A. *Methods in Molecular Medicine*. **2004**, *98*,9.
528   (36)   Rogniaux, H. Sanglier, S. Strupat, K. Azza, S. Roitel, O. Ball, V. Tritsch, D. Branlant, G.
529   Van Dorsselaer, A. *Anal. Biochem.* **2001**, *291*, 48.
530   (37)   Chowdhury, S. K. Katta, V. Chait, B. T., *J. Am. Chem. Soc,* **1990**, *112*, 9012.
531   (38)   Katta, V. Chait, B. T. *J. Am. Chem. Soc.,* **1991**, *113*, 8534.
532   (39)   Cubrilovic, D. Zenobi, R. Anal. Chem. **2013**, 85, 2724.
533   (40)   Benesch, J. L. Robinson, C. V. *Curr. Opin. Struct. Biol.* **2006**, *16*, 245.
534   (41)   Bryngelson, J. D. Onuchic, J. N. Socci, N. D. Wolynes, P. G. *Proteins: Structure, Function,*
535   *and Bioinformatics* **1995**, *21*, 167.
536   (42)   Narhi, L. O. Philo, J. S.Li, T. Zhang, M. Samal, B. Arakawa, T. *Biochemistry* **1996**, *35*,
537   11447.
538   (43)   Jecklin, M. Touboul, D. Bovet, C. D. Wortmann, A. Zenobi, R. *J. Am. Soc. Mass Spec.,*
539   **2008**, *19*, 332.
540   (44)   Petros, A. M. Nettesheim, D. G. Wang, Y. Olejniczak, E. T. Meadows, R. P. Mack, J.
541   Swift, K. Matayoshi, E. D. Zhang, H. Fesik, S. W. Thompson, C. B. *Protein Science*
542   **2000**, *9*, 2528.
543   (45)   Vogler, M. Furdas, S. D. Jung, M. Kuwana, T. Dyer, M. J. S. Cohen, G. M. *Clin. Cancer*
544   *Res.,* **2010**, *16*, 4217.

545
546
547
548
549
550
551
552
553   **Tables and Figures**

554

555
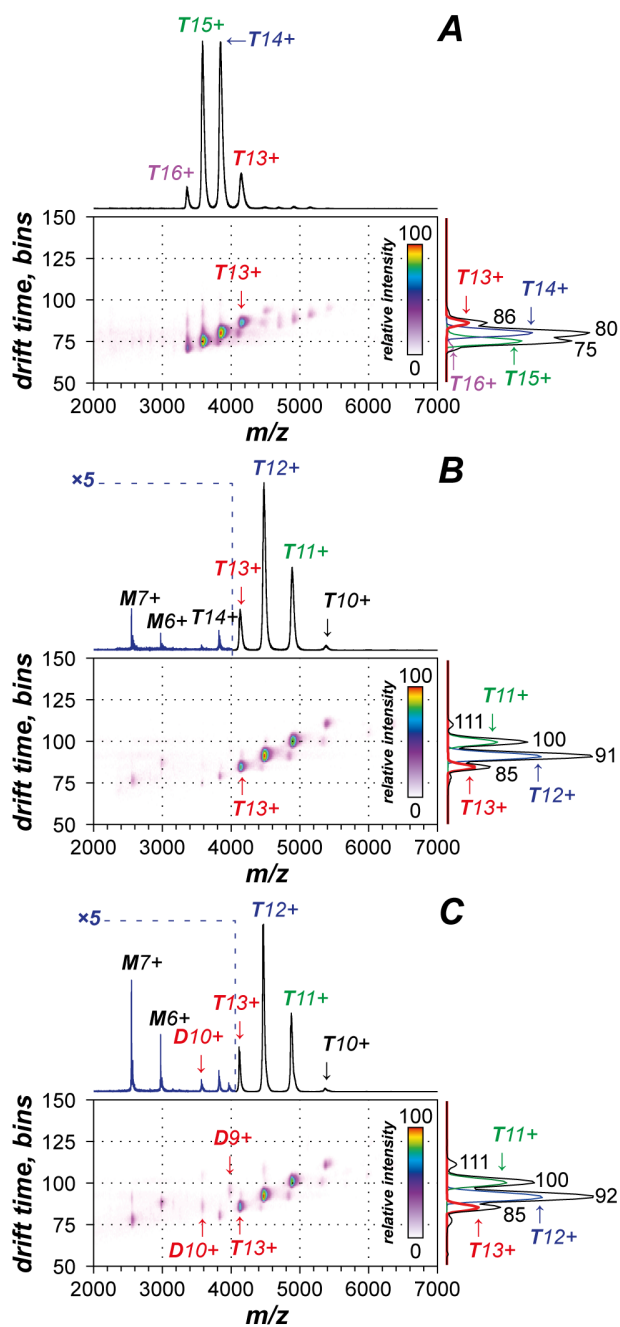
Figure 1. IMS-MS analysis of TNF-alpha under native ESI-MS conditions. Shown are 2D IMS drift time vs. *m/z* plots with corresponding mass spectra (top traces) and drift time distributions (traces on the right). Peaks corresponding to monomeric, dimeric, and trimeric TNF-alpha ions are labelled as *M*, *D*, and *T*, respectively, and their charge states are indicated. Peak maxima in the drift time distributions are labelled with the respective bin numbers. Along with the integral drift time distributions (black traces), some selected-ion drift time distributions are shown in

562   color. Peak labels are color-coded accordingly. **A.** 4.5 μM TNF-alpha solution in 75 mM

563   ammonium acetate buffer pH 7.7. **B.** Same as in **A**, but in the presence of 1 % (vol.) DMSO: note

564   the overall charge state reduction and the appearance of a small amount of monomers **C.** Same as

565   in **A**, but in the presence of 1 % (vol.) DMSO and 100 μM SPD304: note the appearance of dimer

566   ions and the increase of monomer peak intensities. Parts of the mass spectra in B and C are

567   shown at 5-fold magnification.

568

569

570

571

572

573

574

575

576

577

578

22

579
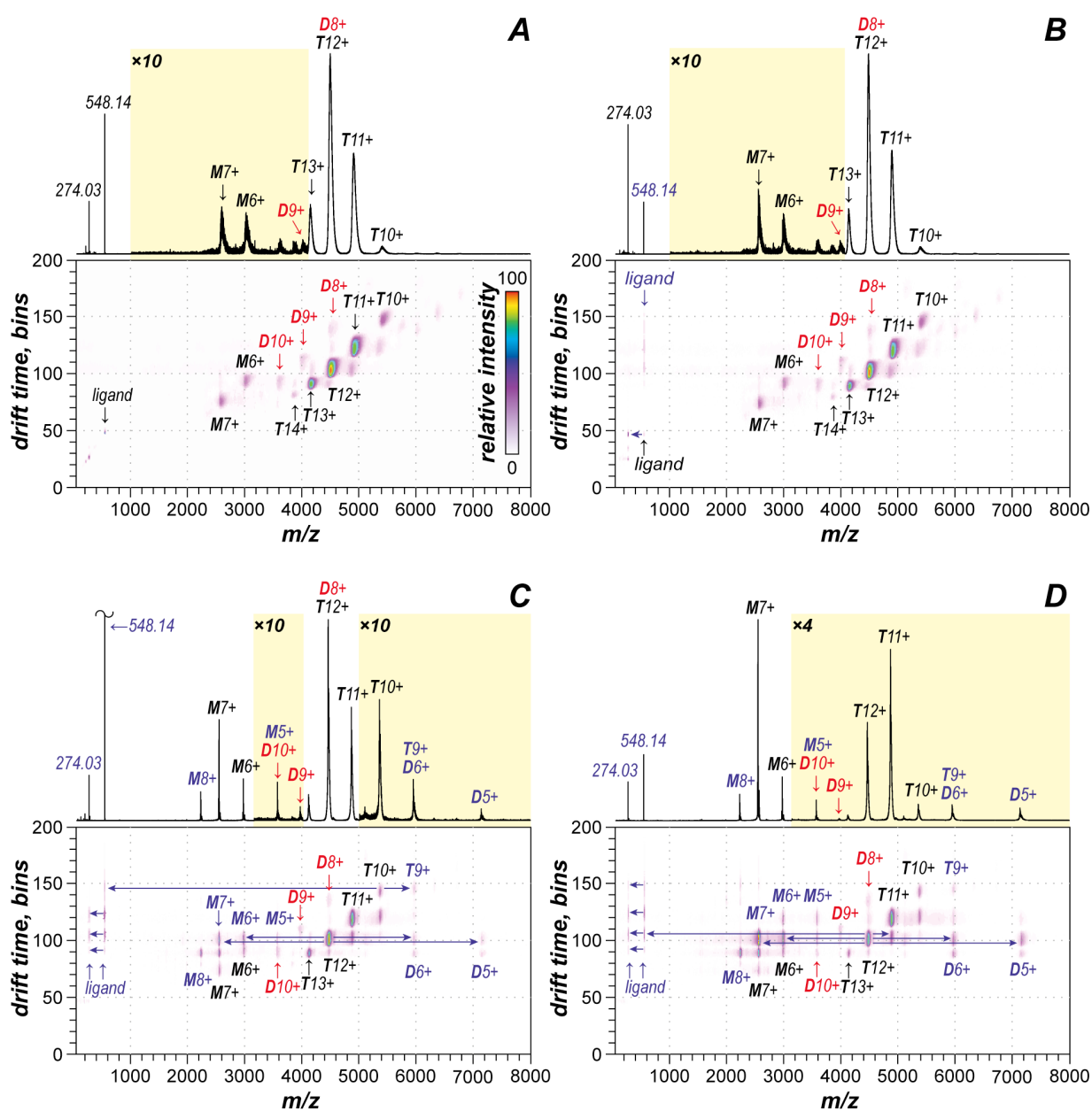
Figure 2. IMS-MS analysis of TNF-alpha ions produced under "native ESI" conditions from
4.5 μM protein solution in 75 mM ammonium acetate buffer (pH 7.7) containing 1 % (vol.)
DMSO and 100 μM SPD304 (marked as ligand). The samples were analyzed at various transfer
collision energy offsets: 5 V (A), 30 V (B), 90 V (C), and 130 V (D). Peaks corresponding to
monomeric, dimeric, and trimeric TNF-alpha ions are marked as M, D, and T, respectively, and
their charge states are assigned. Note the presence of TNF-alpha dimer ions D8+, D9+, and D10+
(marked in red) even at low transfer collision energy offsets (A, B). At high collision energy
offsets (C, D), collision-induced dissociation (CID) of TNF-alpha ions occurred in the transfer

23

588   region of the mass spectrometer, after IMS separation (fragments marked with blue text). Thus,

589   fragment ions have the same drift time, as the respective parent ions (some dissociation channels

590   are indicated with blue arrows). Note that D8+, D9+, and D10+ ions have their own characteristic

591   drift time distributions, which are different from those of the dimer ions originating in the gas

592   phase due to CID. Therefore, D8+, D9+, and D10+ ions must have been present in the sample

593   prior to IMS-MS analysis, i.e. they occurred due to SPD304-promoted dissociation of TNF-alpha

594   trimers in solution.

595

596

597

598

599

600

601

602

603

604

605

606

607
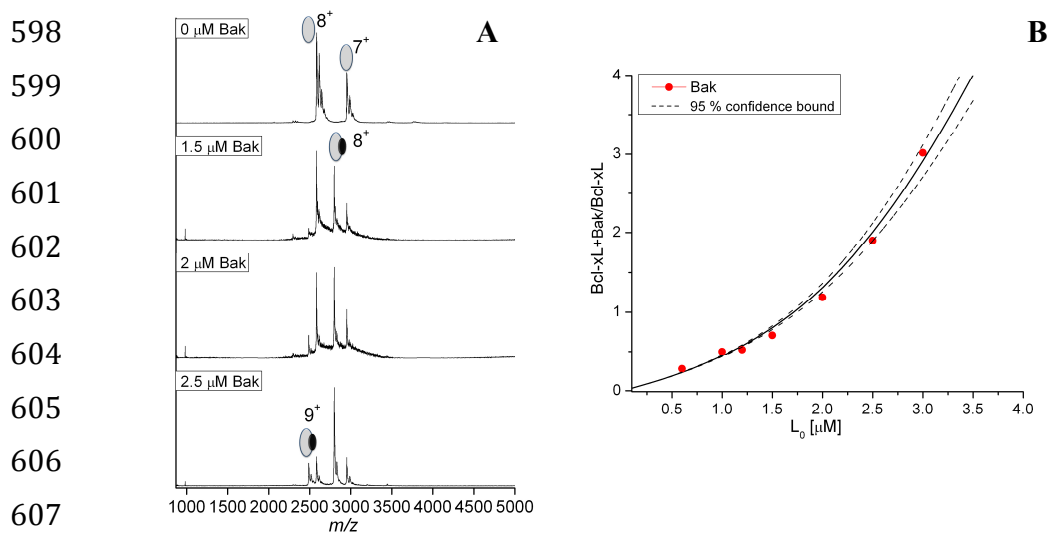
608

609   **Figure 3. A.** Representative nanoESI mass spectra of 3 μM Bcl-x_L in complex with Bak (filled

610   circle) obtained in positive ion mode under "native" conditions. In the first spectrum adduct

611   formation due to the small residue of HEPES buffer is detected. Titration experiments are shown

612   adding different Bak concentration to the Bcl-x_L. The signal for the noncovalent complex clearly

613   increases with increasing Bak concentration present in solution. **B**. NanoESI-MS titration curves

614   for Bcl-x_L•Bak complex. The Bak concentration ranges from 0.5 to 3 μM, while the protein
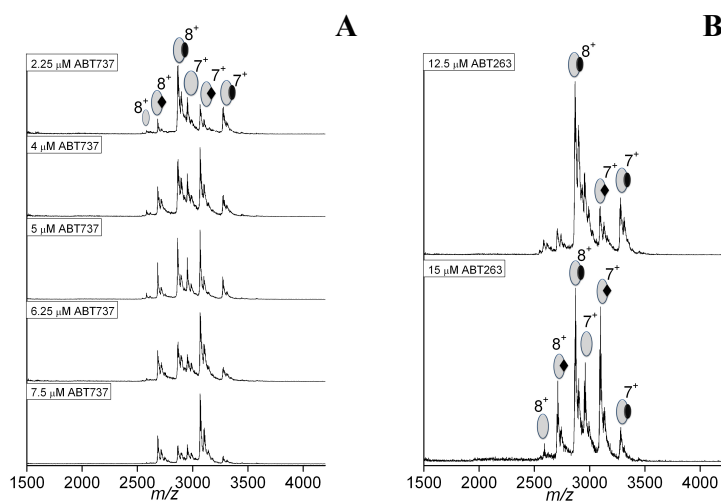
615   concentration was kept constant.

616

617

618

619
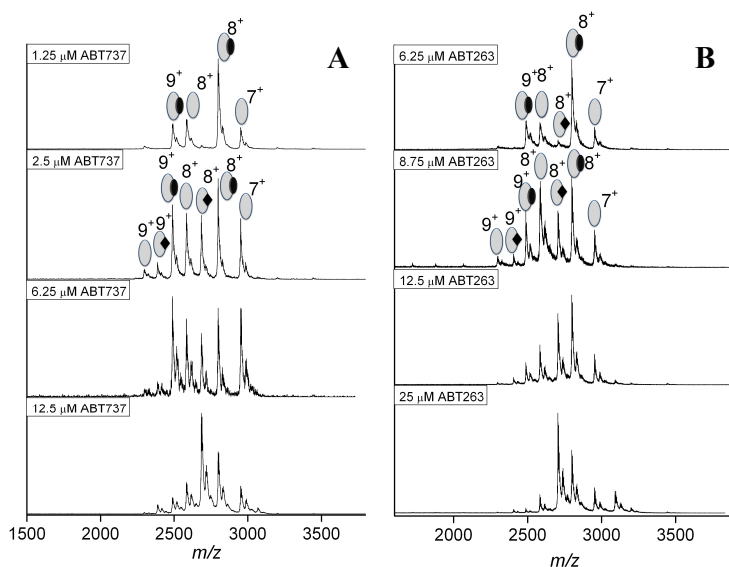
Figure 4. NanoESI mass spectra of 3 μM Bcl-x$_L$ in complex with 3 μM Bak (filled circle) in the presence of different concentrations of small disruptor (filled rhombus) **A.** ABT737 and **B.** ABT263. The heterodimer signal clearly decreases with increasing inhibitor concentration present in solution.

Figure 5. NanoESI mass spectra of 3 μM Bcl-x$_L$ in complex with 20 μM Bad (filled circle) in the presence of different concentration of small disruptor (filled rhombus) **A.** ABT737 and **B.** ABT263

25

652
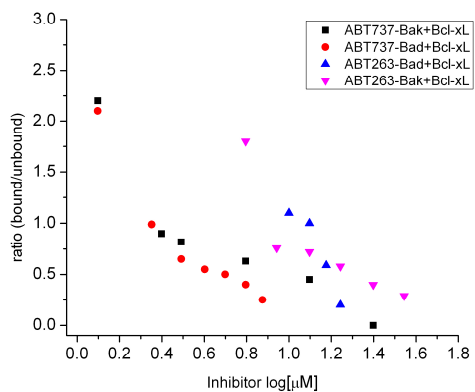
Figure 6. Plotted ratios (bound heterodimers/ unbound bare Bcl-x$_L$ and Bcl-x$_L$-ABT737

complex) against the different inhibitor concentration in order to dissociate the heterodimer

655

656

657

658

659

660

661

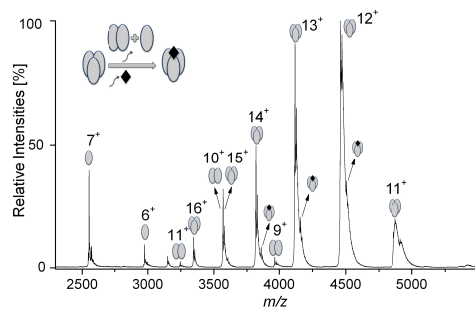662

663

664

665

666

667

668

669

670

671

672

673

674

675

676 **TOC**

677

678
679   We investigated the inhibition of the protein–protein interactions by nanoESI-MS to

680   monitor the extent of inhibition and binding mechanism.